

# RSC Advances



This is an *Accepted Manuscript*, which has been through the Royal Society of Chemistry peer review process and has been accepted for publication.

*Accepted Manuscripts* are published online shortly after acceptance, before technical editing, formatting and proof reading. Using this free service, authors can make their results available to the community, in citable form, before we publish the edited article. This *Accepted Manuscript* will be replaced by the edited, formatted and paginated article as soon as this is available.

You can find more information about *Accepted Manuscripts* in the [Information for Authors](#).

Please note that technical editing may introduce minor changes to the text and/or graphics, which may alter content. The journal's standard [Terms & Conditions](#) and the [Ethical guidelines](#) still apply. In no event shall the Royal Society of Chemistry be held responsible for any errors or omissions in this *Accepted Manuscript* or any consequences arising from the use of any information it contains.



Journal Name

ARTICLE

## Photocatalytic oxidation of small molecule hydrocarbons over Pt/TiO<sub>2</sub> nanocatalysts

Received 00th January 20xx,  
Accepted 00th January 20xx

DOI: 10.1039/x0xx00000x

www.rsc.org/

Yunpeng Li,<sup>ab</sup> Yuanzhu Cai,<sup>a</sup> Xuxing Chen,<sup>a</sup> Xiaoyang Pan,<sup>a</sup> Mingxue Yang<sup>a</sup> and Zhiguo Yi\*<sup>a</sup>

High active Pt/TiO<sub>2</sub> catalysts were prepared by a simple photo-reduction method and used for catalytic oxidation of alkanes (C<sub>2</sub>H<sub>6</sub> and C<sub>3</sub>H<sub>8</sub>) and alkenes (C<sub>2</sub>H<sub>4</sub> and C<sub>3</sub>H<sub>6</sub>). It was found that, significantly improved photo-activity can be reached even by loading a very small amount of Pt (0.2-0.5 wt%). Moreover, the Pt loading resulted in unexpectedly visible light activity for the oxidation of small molecule hydrocarbons. Further investigation using photoluminescence spectra indicate that the Pt loading help reducing the charge carrier recombination within the TiO<sub>2</sub> nanoparticles. Electron Paramagnetic Resonance (EPR) spectra reveal both oxygen molecule and lattice oxygen participate in the hydrocarbons' photooxidation. The transfer and reaction mechanism of charge carriers during the photo-oxidation process were carefully discussed.

### Introduction

The environmental impact of atmospheric hydrocarbons (HC) that released from human activities is receiving increasing attention<sup>1-4</sup>. On one hand, the presence of HC in the environment has an adverse effect on human health. Prolonged exposure can cause damage to the central nervous system. In certain conditions it can generate irritating photochemical smog as well as other more noxious compounds. On the other hand, HC is greenhouse gas and methane has been recognized to be a major contributor to global warming. Therefore, it is imperative to develop techniques to treat HC pollutants in the atmosphere.

Taking into account the effluent HC released from human activities usually feature with low concentration and high flow volume, thermally catalytic oxidation of the HC species is costly<sup>5-6</sup>. Adsorption is a cheaper alternative,<sup>7</sup> however, it is less active for small molecule hydrocarbons. In general, small molecule hydrocarbons such as methane, ethane, propane, etc., are one of the least reactive of all volatile organic compounds (VOCs) owing to their high C-H bond energy and weak molecule polarity, thus making their oxidation a highly energy intensive process. With these aspect in view, heterogeneous photocatalysis using semiconductors is a

potentially important strategy in the removal of low level HC pollutants.

For photocatalytic oxidation of HC species, the generation of the active oxygen species O<sub>2</sub><sup>-</sup> and •OH radicals is crucial step. Semiconductors with a conduction band minimum higher than the potential of O<sub>2</sub>/O<sub>2</sub><sup>-</sup> (-0.16 V vs. NHE<sup>8</sup>) and valence band maximum lower than the •OH/OH<sup>-</sup> (+2.59 V vs. NHE<sup>9</sup>) potential is needed for organic pollutant degradation. TiO<sub>2</sub>, whose conduction band and valence band located at -0.29 eV and 2.91 eV respectively, was widely used in the process of environmental cleanup.<sup>10-15</sup> For example, Izumi, I. et al reported the photocatalytic activities of Pt/P25 for benzene decomposition in aqueous solution<sup>16</sup>. F.B. Li et al investigated the photocatalytic oxidation of methylene blue (MB) and methyl orange (MO) in aqueous solutions using the Pt-TiO<sub>2</sub> catalyst<sup>17</sup>. Wang et al obtained highly dispersed platinum (Pt) nanoparticles embedded in a cubic mesoporous nanocrystalline anatase (meso-ncTiO<sub>2</sub>) thin film and tested its catalytic activity in oxidation of CO<sup>18</sup>. Yu et al fabricated Pt/TiO<sub>2</sub> nanosheets with exposed (001) facets and investigated its activity in photocatalytic water splitting<sup>19</sup>. Wang, C. C. et al prepared uniformly dispersed Pt nanoparticles on TiO<sub>2</sub>-based nanowires and investigated its activity in degradation of rhodamine B and hydrogen evolution<sup>20</sup>. Brigden, C. T. et al<sup>21</sup> studied the UV-induced photo-oxidation of propene, propane, ethene, ethane, *n*-butane and *n*-hexane over a TiO<sub>2</sub> photocatalyst at 150°C. Finger, M. et al<sup>22</sup> reviewed previous reports and discussed the kinetics and mechanisms of photocatalyzed total oxidation reaction of HC species with TiO<sub>2</sub> in the gas phase. Van der Meulen, T. et al<sup>23</sup> studied the photocatalytic oxidation of propane on anatase, rutile, and mixed-phase anatase–rutile TiO<sub>2</sub> nanoparticles. However, photo-oxidation of small molecule alkanes and alkenes using Pt/TiO<sub>2</sub> catalyst is still lacking. Besides, the transfer mechanism of electrons and

<sup>a</sup> Key Laboratory of Design and Assembly of Functional Nanostructures & Fujian Provincial Key Laboratory of Nanomaterials, Fujian Institute of Research on the Structure of Matter, Chinese Academy of Science, Fuzhou 350002, China, E-mail: zhiguo@fjirsm.ac.cn; Fax: +86-591-63179176.

<sup>b</sup> College of Material Science and Engineering, Fujian Normal University, Fuzhou 350007, China

† Electronic Supplementary Information (ESI) available: (a) The sketch of photoreaction in a sealed quartz reactor; (b) the schematic diagram of continues flow photocatalytic test; (c) The spectrum of simulated solar light; (d) The visible light spectrum of simulated solar light; (e) The turnover number (TON) calculations. See DOI: 10.1039/x0xx00000x

holes in bulk of Pt/TiO<sub>2</sub> during photo-oxidation of HC remain uncertain.

In light the fact that TiO<sub>2</sub> is a stable, inexpensive and harmless semiconductor, and, depositing noble metals on the surface of TiO<sub>2</sub> have been proved to be an effective method in improving performance. In this paper, we report photocatalytic activity and photooxidative mechanism of small molecule hydrocarbons over Pt/TiO<sub>2</sub> nanocatalysts. It was found for the first time that, significantly improved photo-activity can be reached even by loading a very small amount of Pt (0.2-0.5 wt %). Moreover, the Pt loading resulted in unexpectedly visible light activity for the oxidation of small molecule hydrocarbons.

## Experimental

**Material** Degussa P25 (BET surface area about 50 m<sup>2</sup>g<sup>-1</sup> and particle size about 20 -30 nm) was purchased from Degussa Corporation, Germany. Methanol (CH<sub>3</sub>OH) and chloroplatinic acid (H<sub>2</sub>PtCl<sub>6</sub>) were all purchased from Sinopharm Chemical Reagent Co., Ltd. All these chemicals were used without further purification and all the water used in this paper was deionized water.

**Synthesis of Pt/P25 photocatalysts** The Pt/P25 powder photocatalysts were prepared by the photo-reduction method, according to the following procedure: First, 1.0 g of P25 was dispersed in 100 ml water and methanol mixture solution (The volume ratio of H<sub>2</sub>O to CH<sub>3</sub>OH equals 7:3). Then, H<sub>2</sub>PtCl<sub>6</sub> solution (0.154 M) with controlled Pt loading amount (0-0.7 wt%) was added into the suspension and magnetically stirred in dark for 3 hours. After that, the suspension was illuminated for 3 hours using a 300 W Xe lamp. The obtained products were filtered, washed and then dried. Finally, the Pt/P25 powders were annealed at 350 °C for 2 hours in vacuum and then cooled naturally to room temperature.

**Characterization** The powder X-ray diffraction (XRD) patterns of the samples were collected on a Miniflex 600 diffractometer with Cu K<sub>α</sub> radiation (λ=0.154178 nm). The morphology and microstructure of the samples were examined by both transmission electron microscopy (TEM) and high-resolution transmission electron microscopy (HRTEM). The UV-Visible absorption spectra of the as-synthesized samples were measured on a UV-Vis-NIR spectrophotometer (Lambda 950), during which BaSO<sub>4</sub> was employed as the internal reflectance standard. A TriStar II3020-BET/BJH surface area analyzer was used to measure the surface area of the samples. Electron Paramagnetic Resonance (EPR) spectra were collected on an ELEXSYS E500 spectrometer equipped with a nitrogen cryostat. All the spectra were collected at 100 K. The photoluminescence (PL) spectra of the photocatalysts were obtained by a Varian Cary Eclipse spectrometer with an excitation wavelength of 325 nm.

**Measurements of photocatalytic activity** The photocatalytic oxidation of hydrocarbons (HC) over the obtained catalysts were evaluated by measuring the decomposition rate of low molecular weight alkanes and alkenes (C<sub>2</sub>H<sub>4</sub>, C<sub>3</sub>H<sub>6</sub>, C<sub>2</sub>H<sub>6</sub>, and

C<sub>3</sub>H<sub>8</sub>) in a sealed quartz reactor of 435 ml capacity (Supporting Information, Figure S1) and a homemade flow-bed pyrex reactor (Supporting Information, Figure S2), respectively. All the experiments were conducted at atmospheric pressure and room temperature.

In a typical fixed-bed reaction: First, 0.2 g of the obtained catalysts were uniformly dispersed on the bottom of a circular glass dish (diameter 60 mm). Then the glass dish was placed in the bottom of the reactor. After that, the reactor was sealed. The initial gas atmosphere was dry air and followed by injection of 200 μL HC gas. Simulated solar light (Supporting Information, Figure S3) was provided by a 300 W Xe lamp. The cut-off filters were employed when visible light (λ>420 nm, Supporting Information, Figure S4) illumination was in demand. At a certain time interval, 4 ml of reactor gas was sampled and analyzed on a gas chromatograph (GC9720 Fuli) equipped with a HP-Plot/U capillary column, a molecular sieve 13X column, a flame ionization detector (FID) and a thermal conductivity detector (TCD).

The continuous flow photocatalytic tests of the samples were carried out in a flow reactor (Figure S2): Typically, the catalysts were first experienced pelleting and sieving to obtain particle size in the range of 0.15-0.2 mm. Then 0.5 g of the particles were filled into a quartz reactor (28 mm × 18 mm × 1 mm) and flowing N<sub>2</sub> was used to expel CO<sub>2</sub> and other species that adsorbed on the surface of the catalysts. After that, the mixed gas consisted of 78.9% N<sub>2</sub>, 21.1% O<sub>2</sub> and small quantity of HC was flowed through the samples and analyzed directly by the gas chromatography (GC9720 Fuli). During the reaction, a 300 W Xe lamp was used to provide simulated solar light.

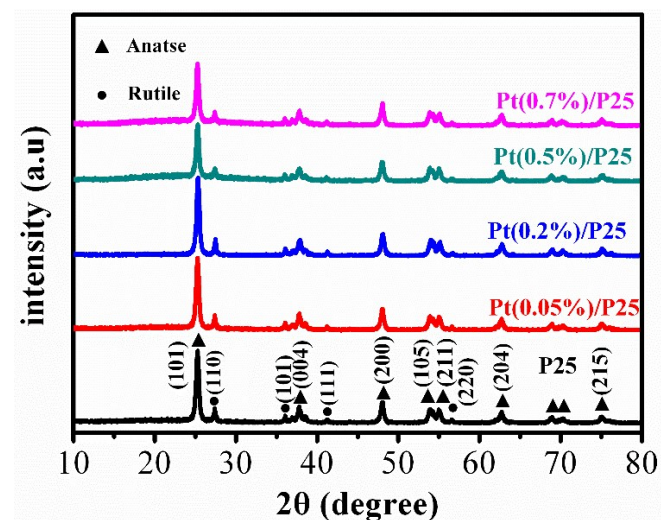


**Fig. 1** The powder XRD patterns of the Pt loaded P25 samples with different weight percentage.

## Results and discussion

The powder XRD patterns of P25 and the as-prepared Pt/TiO<sub>2</sub> samples are shown in Figure 1. All the diffraction peaks for all

samples can be assigned to either anatase (JCPDS, No. 21-1272) or rutile (JCPDS, No. 21-1276) phase of  $\text{TiO}_2$ . The fact that no diffraction peaks of Pt was detected is ascribed to its low loading amount ( $< 0.7$  wt %) as well as its good dispersity<sup>24-26</sup>. As shown in Figure 2, TEM and HRTEM observation revealed small Pt nanoparticles ( $\sim 5$  nm) deposited on the surface of  $\text{TiO}_2$  particles ( $\sim 30$  nm) with a high dispersion. The lattice fringes of 0.223, 0.352 and 0.190 nm in the HRTEM image (Figure 2b) are assigned to the (111) plane of  $\text{Pt}^{16}$ , the (101) and (200) planes of anatase- $\text{TiO}_2$ , respectively.

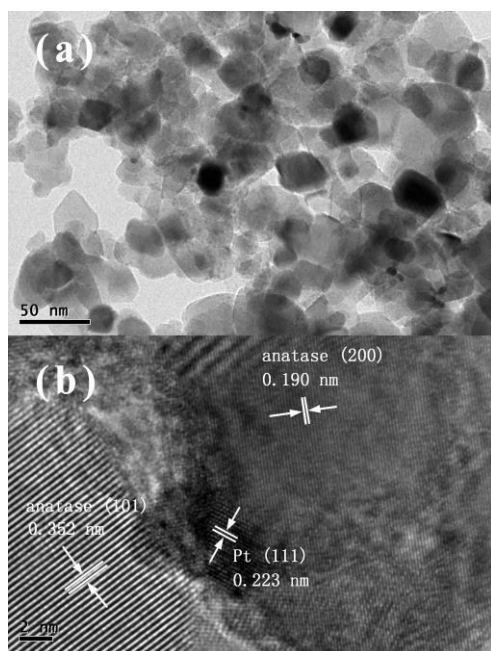


Fig. 2 TEM (a) and HRTEM (b) images of the Pt (0.5 wt %) /P25 sample.

Figure 3a shows the images and UV-Vis absorbance spectra of P25 and the Pt/P25 powders. For all the samples, a particularly strong absorption at wavelengths shorter than 400 nm is attributed to the intrinsic bandgap absorption of anatase  $\text{TiO}_2$  ( $\sim 3.2$  eV). The band gap energy ( $E_g$ ) of the samples was estimated from the intercept of the tangents to the plots of  $(A\text{h}\nu)^2$  vs  $h\nu$ . As shown in Figure 3b, with the increase of Pt, the band gap slightly decreases from 3.25 eV to 3.16 eV. Besides the narrow intrinsic bandgap, note that the Pt loading significantly increased the visible light absorption of P25. Moreover, the absorption intensity increases with increasing the mass fraction of Pt. Accompanying these changes, the colour of the samples changes gradually from white to grey and to black for the 0.0%, 0.05% and 0.7% Pt loaded P25 samples, respectively. The obvious visible light absorption is well corresponding to the excellent activity under irradiation of visible light.

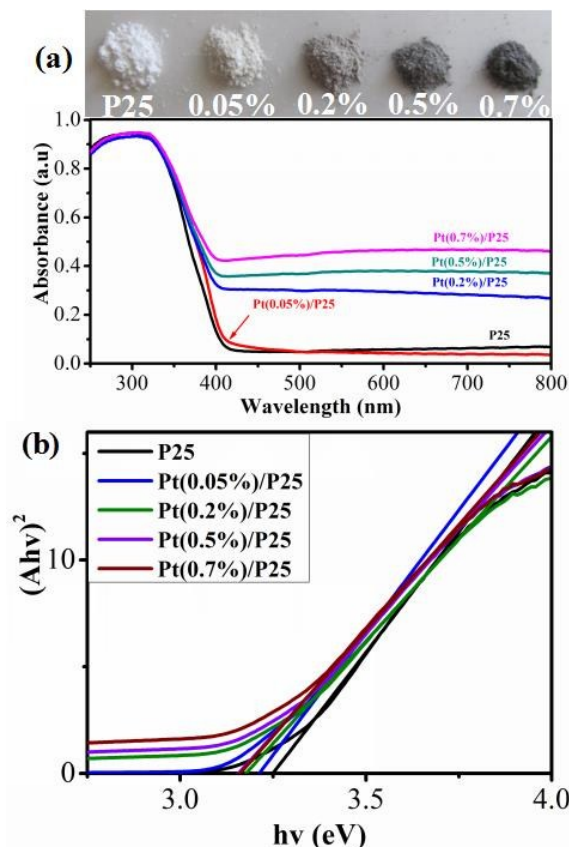


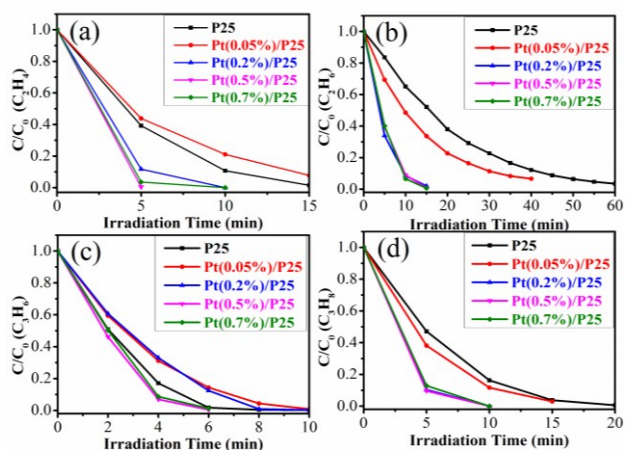
Fig. 3 The images and UV-Vis absorbance spectra (a) as well as the plots of  $(A\text{h}\nu)^2$  vs  $h\nu$  (b) of the Pt loaded P25 samples with different weight percentage.

Figure 4 shows the photocatalytic oxidation of  $\text{C}_2\text{H}_4$ ,  $\text{C}_2\text{H}_6$ ,  $\text{C}_3\text{H}_6$  and  $\text{C}_3\text{H}_8$  over P25 and the as prepared Pt/P25 catalysts under simulated solar light irradiation. The initial concentration of HC in every experiment was  $\sim 450$  ppm. The results indicated that the activity of P25 could be significantly enhanced by loading appropriate Pt in oxidizing both alkenes and alkanes. For the oxidation of alkenes (Figure 4 a and c), 0.5 wt % Pt loading exhibited the highest performance. 450 ppm  $\text{C}_2\text{H}_4$  and  $\text{C}_3\text{H}_6$  could be completely oxidized within 5 and 6 minutes, respectively, under the simulated solar light irradiation. However, for the oxidation of alkanes (Figure 4 b and d), the samples with Pt content of 0.2%, 0.5% and 0.7% showed less distinction. The activity of these samples was enhanced about 4 and 2 times for oxidizing  $\text{C}_2\text{H}_6$  and  $\text{C}_3\text{H}_8$ , respectively, in comparison with P25. The further analysis of the photo-oxidation reaction of HC indicated that all the reactions follow first order reaction kinetics. The rate constant  $k$  in photo-oxidation reaction of HC was listed in Table I. The lower  $k$  values for alkanes ( $\text{C}_2\text{H}_6$  and  $\text{C}_3\text{H}_8$ ) than that for alkenes ( $\text{C}_2\text{H}_4$  and  $\text{C}_3\text{H}_6$ ) is consistent with the understanding that alkanes are more difficult to decompose. That the  $k$  values for the 0.05% Pt samples is lower than that of pure P25 can be understood as follows: The fabrication of the Pt/P25 samples involves processing P25 in water and methanol mixture solution, which may cause the decrease of active sites from P25. When the Pt loading fraction is very low (0.05 wt%), the

increased active sites from Pt deposition can't offset the decrease of active sites from P25.

**Table 1** The BET surface area and rate constant  $k$  in photo-oxidation reaction of P25 and the Pt/P25 samples.

sample	BET (m <sup>2</sup> /g)	Rate constant $k$ (min <sup>-1</sup> )			
		C <sub>2</sub> H <sub>4</sub>	C <sub>2</sub> H <sub>6</sub>	C <sub>3</sub> H <sub>6</sub>	C <sub>3</sub> H <sub>8</sub>
P25	45.6	0.28	0.06	0.69	0.26
Pt(0.05%)/P25	48.2	0.17	0.07	0.47	0.24
Pt(0.2%)/P25	48.9	0.43	0.26	0.64	0.45
Pt(0.5%)/P25	50.5	1.09	0.32	0.91	0.47
Pt(0.7%)/P25	45.8	0.67	0.34	0.75	0.41



**Fig. 4** Photocatalytic oxidation of some small molecule hydrocarbons over P25 and the as-prepared Pt/P25 catalysts under simulated solar light irradiation: (a) C<sub>2</sub>H<sub>4</sub>; (b) C<sub>2</sub>H<sub>6</sub>; (c) C<sub>3</sub>H<sub>6</sub> and (d) C<sub>3</sub>H<sub>8</sub>.

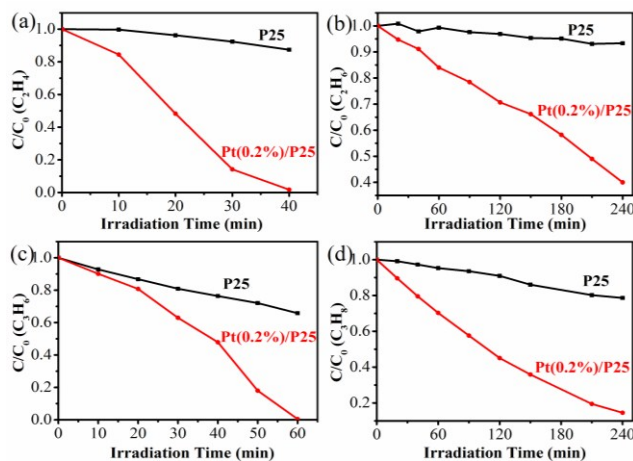


**Fig. 5** Time course of HC oxidation upon P25 and the Pt(0.2%)/P25 powders under the irradiation of visible light: (a) C<sub>2</sub>H<sub>4</sub>; (b) C<sub>2</sub>H<sub>6</sub>; (c) C<sub>3</sub>H<sub>6</sub> and (d) C<sub>3</sub>H<sub>8</sub>.

Because loading Pt nanoparticles on the surface of P25 could significantly increase visible light absorption (Figure 3), the photo-oxidation activity of Pt/P25 under visible light was evaluated as well. Figure 5 shows photooxidation of C<sub>2</sub>H<sub>4</sub>, C<sub>2</sub>H<sub>6</sub>, C<sub>3</sub>H<sub>6</sub> and C<sub>3</sub>H<sub>8</sub> over P25 and the Pt (0.2%)/P25 sample under the visible light irradiation. The results indicated that P25 exhibits very weak visible light activity under the function of its bulk and surface defects. However, for the Pt (0.2%)/P25

sample, significantly increased visible light activity was realized. The 450 ppm of alkenes (C<sub>2</sub>H<sub>4</sub> and C<sub>3</sub>H<sub>6</sub>) was completely degraded within 1 hour (Figure 5 a and c) and the 450 ppm of C<sub>2</sub>H<sub>6</sub> and C<sub>3</sub>H<sub>8</sub> were degraded more than 60% and 80% (Figure 5 b and d), respectively within 4 hours irradiation.

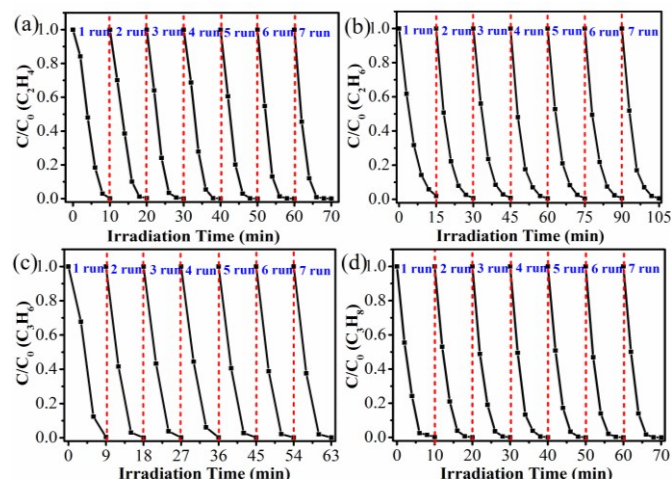


**Fig. 6** Durability tests of the hydrocarbons photo-oxidation upon the Pt (0.2%)/P25 catalysts under the simulated solar light irradiation: (a) C<sub>2</sub>H<sub>4</sub>, (b) C<sub>2</sub>H<sub>6</sub>, (c) C<sub>3</sub>H<sub>6</sub> and (d) C<sub>3</sub>H<sub>8</sub>.

Figure 6 shows durability test of the hydrocarbons photooxidation upon the Pt (0.2%)/P25 catalysts under simulated solar light illumination. For all the HC gases, within seven cycle reactions, the very stable performance indicated that the as-prepared Pt/P25 catalysts are very stable in the processing of HC photo-oxidation.

To examine the mineralization rate, we carried out a flow mode (Figure S2) test on the Pt (0.2%)/P25 catalysts. Before illumination, CO<sub>2</sub> in the reaction system was removed by flowing carrier gas. After that, the reaction gas consisted of 78.9% N<sub>2</sub>, 21.1% O<sub>2</sub> and a small quantity of HC was flowed through the samples and analyzed directly by the gas chromatography (GC9720 Fuli). During the reaction, a 300 W Xe lamp was used to provide simulated solar light with light density of ~200 mW cm<sup>-2</sup>. Figure 7 shows the time courses of C<sub>2</sub>H<sub>6</sub> and C<sub>3</sub>H<sub>8</sub> photooxidation upon the as-synthesized Pt (0.2%)/P25 catalysts under simulated sunlight illumination in the flow mode experiment. Before light was turned on, the concentration of HC was 70 and 205 ppm for C<sub>2</sub>H<sub>6</sub> and C<sub>3</sub>H<sub>8</sub> respectively and no CO<sub>2</sub> was detected. When the lamp is turned on, the amount of ethane and propane decreases rapidly to 0-5 ppm. Simultaneously, the concentration of CO<sub>2</sub> increases promptly to ~140 and ~610 ppm, respectively. The generation of CO<sub>2</sub> was basically in line with the degradation of HC and no other carbon-containing species were detected. When the light is turned off, the concentration of CO<sub>2</sub> rapidly decreases to zero; moreover, the amount of ethane and propane comes back to a constant value. These results confirmed that the HCs oxidation is truly driven by a photodriven process. Besides, under the presence of plenty oxygen, HC tends to totally convert to carbon dioxide. What's

more, the activities of the sample have no decrease after 20 hours irradiation, which evidence again high stability of the Pt/P25 catalysts.

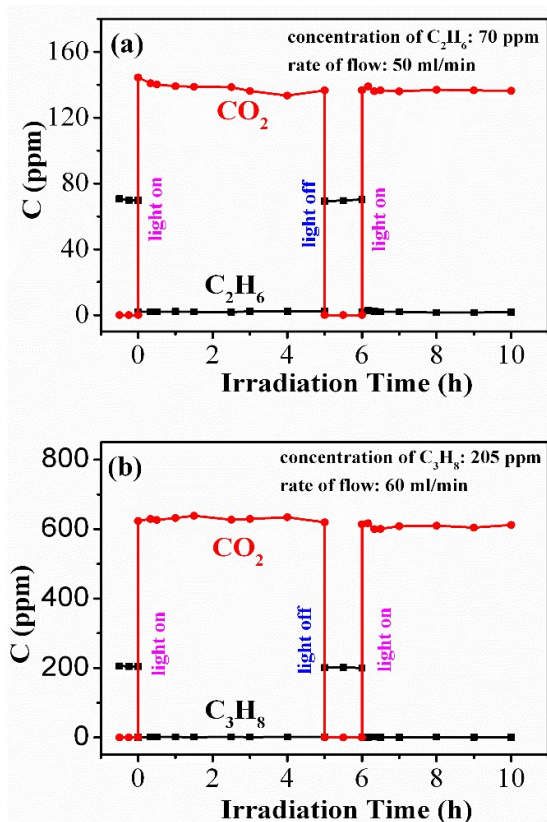


**Fig. 7** Time courses of the HC photooxidation upon the as-synthesized Pt (0.2%)/P25 samples under simulated sunlight illumination in the flow mode (mass of sample: 0.5 g; size of sample particle: 0.15–0.2 mm; one 300 W Xe lamp; reactor size: 28 mm×18 mm×1 mm).

Turnover number (TON) of the HC photo-oxidation was obtained by oxidizing a larger amount of HC gases (10 ml) upon the Pt (0.2%)/P25 catalysts (Figure 8). The calculated TON (supporting information S5) for the HC photo-oxidation was 2.18 for  $C_2H_4$ , 2.55 for  $C_2H_6$ , 3.23 for  $C_3H_6$  and 3.64 for  $C_3H_8$ , respectively, which indicated that the photo-oxidation reaction was truly driven by a catalytic process.

The BET surface areas of P25 and the Pt/P25 samples were summarized in Table I. All the Pt/P25 samples have similar BET surface area with that of P25. Therefore, the increased HC photooxidation activity is obviously correlated with the loading of Pt. One of the benefit is loading of noble metal nanoparticles on the surface of semiconductor could significantly enhance the separation rate of photo-generated electrons and holes<sup>27–28</sup>, which can be examined from the changes of the intensity of photoluminescence (PL) spectra. Lower intensity of PL spectra corresponds to lower recombination rate of photogenerated electron-hole pairs, thus corresponding to higher activity of catalyst<sup>29</sup>. Figure 9 shows the room-temperature PL spectra of P25 and the Pt (0.2%)/P25 catalysts under excitation wavelength of 325 nm. The PL peak at about 400 nm is attributed to the emission

close to bandgap transition with the energy of light approximately equal to or larger than the bandgap energy of anatase (3.2 eV) and rutile (3.0 eV) whereas the broad extension to the visible light range might be correlate with the surface and bulk defects of  $TiO_2$ <sup>19</sup>, which will be discussed later. After Pt nanoparticles decorated on the surface of P25, the fluorescence intensity was obviously decreased compare to pure P25. This result indicates that Pt nanoparticles on P25 surface are able to extract electrons from the conduction band of  $TiO_2$  and thus reduce charge carrier recombination within  $TiO_2$  nanoparticles.

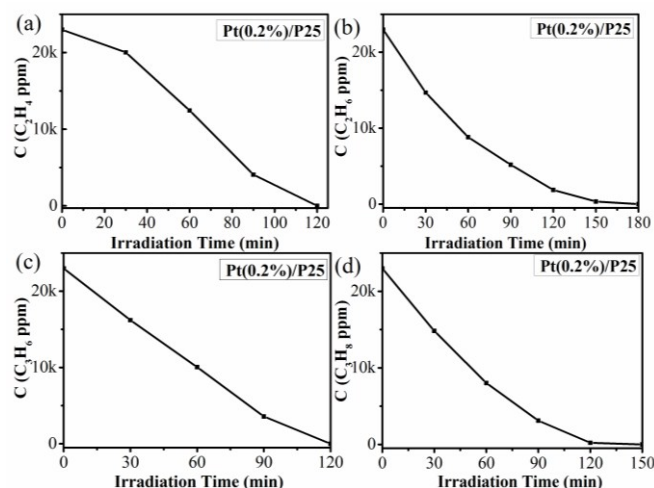


**Fig. 8** photo-oxidation of 10 ml HC upon the Pt (0.2%)/P25 (catalyst: 0.2 g, reactor: 435 ml, reaction gas: 10 ml HC and 425 ml air).

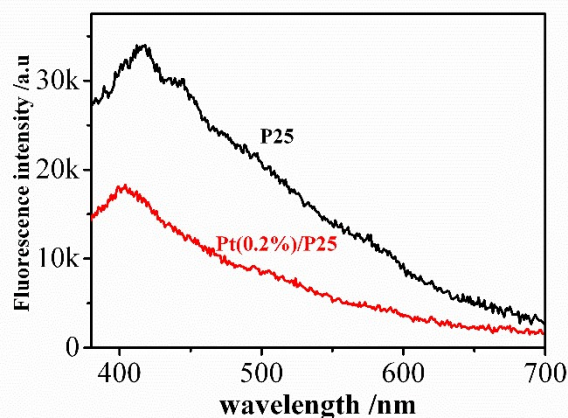


**Fig. 9** the room-temperature PL spectra of P25 and the Pt (0.2%)/P25 catalysts under excitation wavelength of 325 nm.

In order to study the mechanism of electron transfer in the HC photo-oxidation process, we performed the EPR measurements at 100 K over the Pt (0.2%)/P25 catalysts (Figure 10). Under the dark and air atmosphere, the sample shows two signals with  $g = 2.004$  and  $g = 1.979$  (Figure 10 a). The signal of  $g = 2.004$  has been assigned to the characteristic of single-electron-trapped oxygen vacancies<sup>30–33</sup>. We suppose

that these oxygen vacancies might be created during the process of photo-depositing Pt nanoparticles. The signal with  $g = 1.979$  is attributable to the lattice electron trapping sites ( $\text{Ti}^{3+}$ ) in the bulk of  $\text{TiO}_2$ <sup>34-36</sup>. After irradiated by visible light ( $\lambda > 420$  nm, Figure 10 b), the signal of oxygen vacancy and  $\text{Ti}^{3+}$  were obviously increased. In addition, two new signals with  $g = 2.028$  and  $g = 2.009$  emerged, which are assigned to a trapped hole at the surface oxygen of the  $\text{TiO}_2$  as  $\text{Ti}^{4+}-\text{O}^-$ <sup>35-36</sup>. These results indicate that there were more electrons and holes generated and then the electrons were trapped by oxygen vacancy and  $\text{Ti}^{4+}$ , whereas the holes were trapped by subsurface lattice oxygen. We should note that visible light have no enough energy to excite electrons from valence band to the conduction band of  $\text{TiO}_2$ .

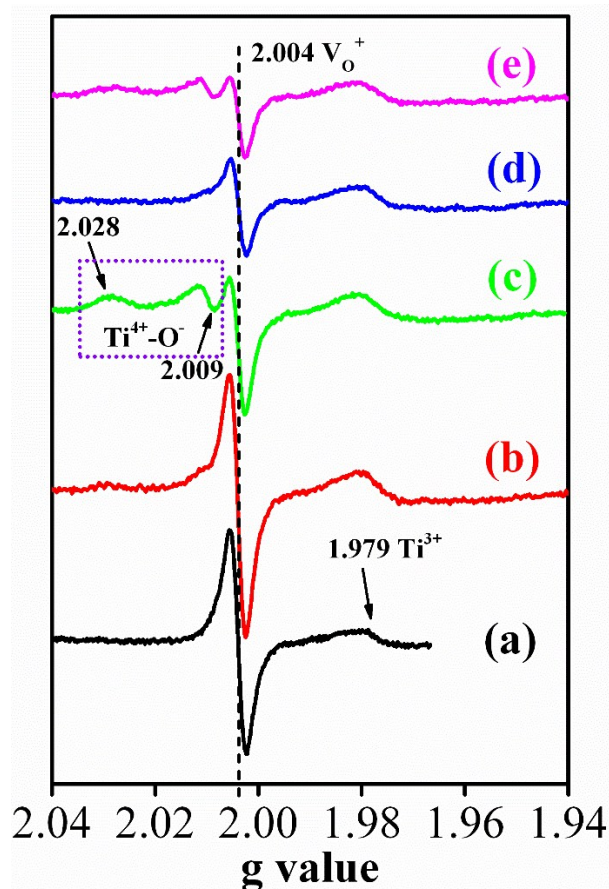


**Fig. 10** EPR spectra collected upon the Pt/P25 sample at 100 K under various conditions: (a) in dark and air atmosphere; (b) irradiated in air atmosphere for 10 min under visible light; (c) irradiated in air atmosphere for 10 min under ultraviolet light; (d) subsequently inject  $\text{C}_2\text{H}_4$  immediately after (c); (e) continue lighting for 10 min under simulated sunlight after the injection of  $\text{C}_2\text{H}_4$ .

However, it was reported that oxygen vacancies generated during synthesis could enhance the visible light activity<sup>30, 37</sup>. Oxygen vacancies should involve in the transfer process of photo-generated electron-hole pairs. According to the earlier reports<sup>38-40</sup>, there should be a two-step electron excitation through the defect level. It had been reported that oxygen vacancy locates at 0.75-1.18 eV below the conduction band

minimum<sup>41</sup>. Therefore, with the irradiation of visible light, electrons in the valence band of  $\text{TiO}_2$  can be excited to the local level of oxygen vacancy and then from there to the conduction band. Note the possibility of electrons transfer directly from the defect level to the adsorbed hydrocarbons cannot be ruled out herein. When irradiated under ultraviolet light (Figure 10 c), the signal of  $\text{Ti}^{4+}-\text{O}^-$  increased significantly; at the same time, the signal of single-electron-trapped oxygen vacancy decreased compared to visible light irradiation. It can be explained as follows: after absorbing ultraviolet light, a lot of electrons and holes were generated. Then, more holes trapped at surface oxygen of the  $\text{TiO}_2$  lead to the increased signal of  $\text{Ti}^{4+}-\text{O}^-$ ; meanwhile, electrons trapped at  $\text{V}_\text{o}^+$  lead to the decreases of its intensity. When  $\text{C}_2\text{H}_4$  was injected into the reactor, as shown in Figure 10 d, the signal of  $\text{Ti}^{4+}-\text{O}^-$  completely disappeared; besides, the signal of  $\text{V}_\text{o}^+$  continue decreases compared to Figure 10 c. This result is due to  $\text{C}_2\text{H}_4$  gives one electron to the surface  $\text{O}^-$  through a still unknown process after it touch with catalyst, result in the disappear of  $\text{Ti}^{4+}-\text{O}^-$ ; besides, the decrease of  $\text{V}_\text{o}^+$  is owing to electrons continue trapping at this sites and form  $\text{V}_\text{o}$ . In order to examine this speculation, the quartz glass tube containing air and  $\text{C}_2\text{H}_4$  was irradiated under simulated sun light for 10 minutes (Figure 10 e), it is not surprise that the signal of  $\text{Ti}^{4+}-\text{O}^-$  emerge again.

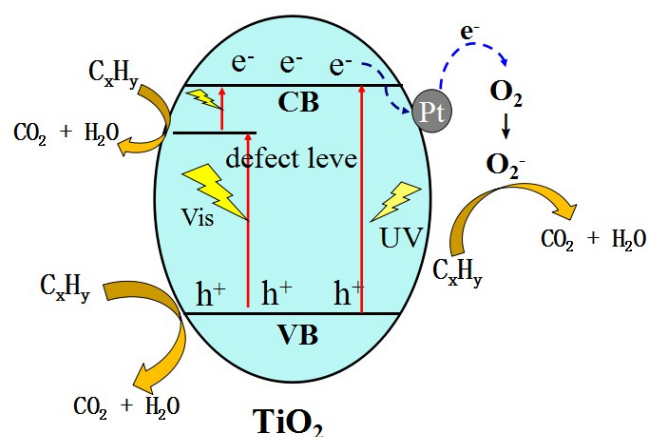
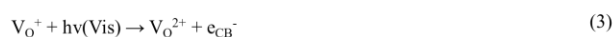
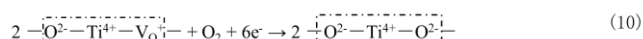
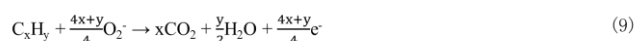
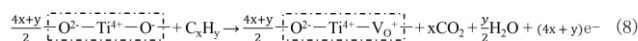
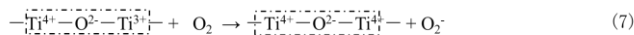
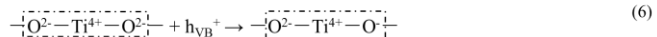
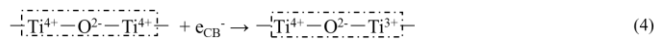


**Fig. 11** suggested mechanism of visible and ultraviolet light induced reaction on the Pt/P25 photocatalyst.

According to the above discussion, the transfer of charge carriers during the HC photooxidation upon the Pt/P25 catalyst is described in Figure 11. During the irradiation of simulated solar light, the absorption of UV photons led to the generation of electron-hole pairs, and, the visible light irradiation will result in two-step electron excitation through the defect levels<sup>38, 42-43</sup>.



Then, in the bulk of TiO<sub>2</sub>, these charge carriers can be trapped at several centers<sup>42-43</sup>. In addition, part of the electrons will transfer to the loaded Pt nanoparticles.



Finally, the trapped electrons and holes transfer to electron acceptor O<sub>2</sub> and electron donor C<sub>x</sub>H<sub>y</sub>. The generated O<sub>2</sub><sup>-</sup> and lattice O<sup>-</sup> reacted with C<sub>x</sub>H<sub>y</sub> to produce carbon dioxide and water (formula 8, 9), then the V<sub>O</sub><sup>+</sup> could be recovered to O<sup>2-</sup> by absorbing oxygen in air (formula 10).

## Conclusions

High active and stable Pt/TiO<sub>2</sub> catalysts were obtained by a facile photo-reduction method and the activity of oxidizing alkanes and alkenes on these catalysts was examined. The results indicate that the photocatalytic activity of P25 could be significantly enhanced by deposition of Pt and the best mass fraction of Pt on P25 is about 0.2-0.5wt%. The transfer mechanism of charge carriers during photo-oxidation process was also investigated and discussed. Photo-generated electrons are trapped by Ti<sup>4+</sup> and then transfer to O<sub>2</sub> in air to form O<sub>2</sub><sup>-</sup>; lattice O<sup>2-</sup> traps one hole to form O<sup>-</sup> and then recover to O<sup>2-</sup> by obtaining one electron from the HC electron donor. The Pt loading as well as the defect such as oxygen vacancy in bulk and surface of TiO<sub>2</sub> should be the main factor responsible for the photo-response under visible light.

## Acknowledgements

This work was financially supported by the National Key Project on Basic Research (Grant No. 2013CB933203), the Natural Science Foundation of China (Grant Nos. 21373224, 21577143 and 51502289), the Natural Science Foundation of Fujian Province (Grant No. 2014H0054 and 2015J05044), and the One Hundred Talents Program of the Chinese Academy of Sciences.

## Notes and references

1 Forster, P.; Ramaswamy, V.; Artaxo, P.; Berntsen, T.; Betts, R.; Fahey, D. W.; Haywood, J.; Lean, J.; Lowe, D. C.; Myhre, G.,

Changes in atmospheric constituents and in radiative forcing. In *Climate Change 2007. The Physical Science Basis*, 2007.

2 Kang, H.; Choi, B.; Son, G.; Foster, D. E., *JSME International Journal Series B Fluids and Thermal Engineering* 2006, **49** (2), 419-425.

3 Cargnello, M.; Jaén, J. D.; Garrido, J. H.; Bakhmutsky, K.; Montini, T.; Gámez, J. C.; Gorte, R.; Fornasiero, P., *Science* 2012, **337** (6095), 713-717.

4 Caillol, S., *J. Photochem. Photobiol., C* 2011, **12** (1), 1-19.

5 Carp, O.; Huisman, C. L.; Reller, A., *Prog. Solid State Chem.* 2004, **32** (1), 33-177.

6 Krishna, V.; Kamble, V. S.; Gupta, N. M.; Selvam, P., *J. Phys. Chem. C* 2008, **112** (40), 15832-15843.

7 Twesme, T. M.; Tompkins, D. T.; Anderson, M. A.; Root, T. W., *Appl. Catal., B* 2006, **64** (3), 153-160.

8 Wood, P. M., *Biochem J* 1988, **253** (1), 287.

9 Koppenol, W.; Liebman, J. F., *J. Phys. Chem.* 1984, **88** (1), 99-101.

10 Fu, X.; Clark, L. A.; Yang, Q.; Anderson, M. A., *Environ Sci Technol* 1996, **30** (2), 647-653.

11 Fox, M. A.; Dulay, M. T., *Chem. Rev.* 1993, **93** (1), 341-357.

12 Hoffmann, M. R.; Martin, S. T.; Choi, W.; Bahnemann, D. W., *Chem. Rev.* 1995, **95** (1), 69-96.

13 Fujishima, A.; Rao, T. N.; Tryk, D. A., *J. Photochem. Photobiol., C* 2000, **1** (1), 1-21.

14 Lee, B.-Y.; Park, S.-H.; Lee, S.-C.; Kang, M.; Park, C.-H.; Choung, S.-J., *Korean J. Chem. Eng.* 2003, **20** (5), 812-818.

15 Woan, K.; Pyrgiotakis, G.; Sigmund, W., *Adv. Mater* 2009, **21** (21), 2233-2239.

16 Izumi, I.; Dunn, W. W.; Wilbourn, K. O.; Fan, F.-R. F.; Bard, A. J., *J. Phys. Chem.* 1980, **84** (24), 3207-3210.

17 Li, F.; Li, X., *Chemosphere* 2002, **48** (10), 1103-1111.

18 Wang, X.; Yu, J. C.; Yip, H. Y.; Wu, L.; Wong, P. K.; Lai, S. Y., *Chem-eur J* 2005, **11** (10), 2997-3004.

19 Yu, J.; Qi, L.; Jaroniec, M., *J. Phys. Chem. C* 2010, **114** (30), 13118-13125.

20 Wang, C.-C.; Hsueh, Y.-C.; Su, C.-Y.; Kei, C.-C.; Perng, T.-P., *Nanotechnology* 2015, **26** (25), 254002.

21 Brigden, C. T.; Poulston, S.; Twigg, M. V.; Walker, A. P.; Wilkins, A. J., *Appl. Catal., B* 2001, **32** (1), 63-71.

22 Finger, M.; Haeger, A.; Hesse, D., *Chem Eng Technol* 2005, **28** (7), 783-789.

23 Van der Meulen, T.; Mattson, A.; Österlund, L., *J. Catal.* 2007, **251** (1), 131-144.

24 Huang, H.; Leung, D. Y., *J. Catal.* 2011, **280** (1), 60-67.

25 Nie, L.; Yu, J.; Li, X.; Cheng, B.; Liu, G.; Jaroniec, M., *Environ Sci Technol* 2013, **47** (6), 2777-2783.

26 Peng, J.; Wang, S., *Appl. Catal., B* 2007, **73** (3), 282-291.

27 Zheng, Y.; Chen, C.; Zhan, Y.; Lin, X.; Zheng, Q.; Wei, K.; Zhu, J., *J. Phys. Chem. C* 2008, **112** (29), 10773-10777.

28 Du, L.; Furube, A.; Hara, K.; Katoh, R.; Tachiya, M., *J. Photochem. Photobiol., C* 2013, **15**, 21-30.

29 Udawatte, N.; Lee, M.; Kim, J.; Lee, D., *ACS Appl. Mat. Interfaces* 2011, **3** (11), 4531-4538.

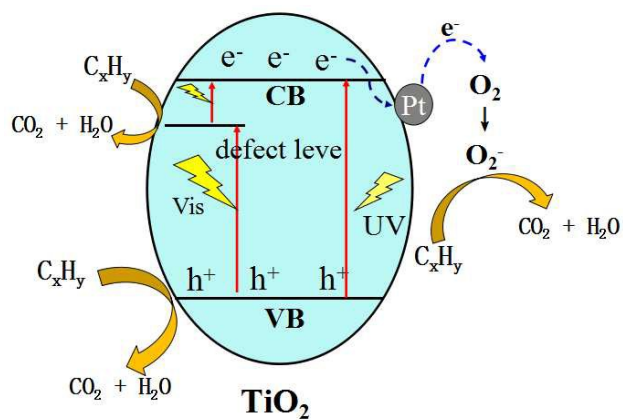
30 Feng, C.; Wang, Y.; Zhang, J.; Yu, L.; Li, D.; Yang, J.; Zhang, Z., *Appl. Catal., B* 2012, **113**, 61-71.

## ARTICLE

Journal Name

- 31 Priebe, J. B.; Karnahl, M.; Junge, H.; Beller, M.; Hollmann, D.; Brückner, A., *Angew. Chem. Int. Ed.* 2013, **52** (43), 11420-11424.
- 32 Nakamura, I.; Negishi, N.; Kutsuna, S.; Ihara, T.; Sugihara, S.; Takeuchi, K., *J. Mol. Catal. A: Chem.* 2000, **161** (1), 205-212.
- 33 Baumann, S. O.; Elser, M. J.; Auer, M.; Bernardi, J.; Hüsing, N.; Diwald, O., *Langmuir* 2011, **27** (5), 1946-1953.
- 34 Hurum, D. C.; Agrios, A. G.; Gray, K. A.; Rajh, T.; Thurnauer, M. C., *J. Phys. Chem. B* 2003, **107** (19), 4545-4549.
- 35 Micic, O. I.; Zhang, Y.; Cromack, K. R.; Trifunac, A. D.; Thurnauer, M. C., *J. Phys. Chem.* 1993, **97** (28), 7277-7283.
- 36 Nishikawa, M.; Sakamoto, H.; Nosaka, Y., *J. Phys. Chem. A* 2012, **116** (39), 9674-9679.
- 37 Li, F.; Li, X.; Hou, M.; Cheah, K.; Choy, W., *Appl. Catal., A* 2005, **285** (1), 181-189.
- 38 Nishikawa, M.; Mitani, Y.; Nosaka, Y., *J. Phys. Chem. C* 2012, **116** (28), 14900-14907.
- 39 Serpone, N.; Emeline, A., *The Journal of Physical Chemistry Letters* 2012, **3** (5), 673-677.
- 40 Tennakone, K.; Bandara, J., *Sol Energ Mat Sol C* 2000, **60** (4), 361-365.
- 41 Cronmeyer, D., *Phys. Rev.* 1959, **113** (5), 1222.
- 42 Howe, R., *Developments in Chemical Engineering and Mineral Processing* 1998, **6** (1 - 2), 55-84.
- 43 Coronado, J. M.; Maira, A. J.; Conesa, J. C.; Yeung, K. L.; Augugliaro, V.; Soria, J., *Langmuir* 2001, **17** (17), 5368-5374.

## Graphical Abstract



The Pt loading over P25 resulted in unexpectedly visible light activity for the oxidation of small molecule hydrocarbons.